Proceedings of
10th European Conference on Turbomachinery Fluid dynamics & Thermodynamics
ETC10, April 15-19, 2013, Lappeenranta, Finland

ASSESSMENT OF NUMERICAL METHODS FOR LOW PRESSURE TURBINE TONE NOISE PREDICTION

L. Pinelli[1] – D. Torzo[2] – F. Poli[1] – A. Arnone[1]

[1]Department of Industrial Engineering
University of Florence, Florence, Italy
Lorenzo.Pinelli@arnone.de.unifi.it

[2]Avio S.p.A. R&D
Rivalta di Torino, Italy
Davide.Torzo@aviogroup.com

ABSTRACT

The capability to accurately predict the tone noise of Low Pressure Turbines (LPT) is crucial in designing and optimizing aircraft engine turbofans for low noise emissions. Especially during approach conditions the LPT is an important noise source for commercial aircraft. In this paper, two methodologies for exhaust turbine tone noise analysis are described and validated against an experimental database measured in an acoustic test rig. The first method, a preliminary analysis technique, is suitable during the early design phase; whereas the second methodology is based on a 3D linearized approach which is used in the last steps of the acoustic design. Very good agreement is observed between numerical predictions and measurements for all interactions at approach operating conditions.

NOMENCLATURE

k	harmonic or scattering index
$\mathscr{K}$	kernel element
k_x, k_y	axial and circumferential wavenumbers
m	circumferential order
N	number of blades
N_p	number of panels
p	disturbance acoustic pressure
$\mathcal{W}$	acoustic power
R	radius
t	time
$\mathscr{L}, \mathscr{W}$	loading and upwash elements
U, V	axial and circumferential components of the mean flow velocity
u, v	axial and circumferential components of the disturbance velocity
W	mean velocity magnitude
x, y	axial and circumferential coordinates
z	chordwise coordinate

Greek:

Γ	vortex strength per chord unit length
Ω	rotational speed
ω	radian frequency
ϱ, ρ	mean and disturbance density
θ	stagger angle

Subscripts:

$_{1,2,3}$	up/downstream pressure, vorticity (b)
$_{4,5,6}$	up/downstream pressure, vorticity (a)
$_{7,8,9}$	up/downstream pressure, vorticity (c)
$_{a,b,c}$	upstream, inter-rows and downstream
$_{\mathrm{f,s}}$	first row, second row

Acronyms:

PWL	sound PoWer Level $= 10\log_{10}(\mathcal{W}/\mathcal{W}_0)$ $\mathcal{W}_0 = 1\,\mathrm{pW}$
SPL	Sound Pressure Level $= 20\log_{10}(p_{\mathrm{rms}}/p_0)$ $p_0 = 20\,\mu\mathrm{Pa}$
V, B	vane, blade

INTRODUCTION

Nowadays, strict legislation on airplane acoustic emissions imposes well defined limits of perceived noise. Such targets can be achieved through an accurate acoustic design and prediction of the whole engine. This procedure includes the analysis of the tonal noise generated inside the turbine, as this component may play an important role in the overall engine acoustic signature at certain operating conditions. For these reasons, the development of fast and reliable numerical techniques to be used both in the preliminary design phase and in the detailed assessments is strongly pushed by the aeronautical industry. Obviously, different design phases require different kinds of tools: fast and

robust techniques for the preliminary choices; accurate and reliable methods for the advanced design verification.

Over the past four decades, countless methods have been developed to predict the acoustic emission at blade passing frequencies. The first major contribution to the aeroacoustics of turbomachinery can be attributed to Tyler and Sofrin (1962), who determined the link between blade count and duct modes and their propagation behavior (cut-on or cut-off). Early methods to compute the strength of these spinning modes were based on analytic models derived from flat plate theory (Amiet (1974); Koch (1971)) where the sound emissions mainly depend on the difference between the wave angle and the stagger angle of the flat plate. Then Ventres et al. (1982) proposed a method which linked a 2D flat plate theory for the unsteady aerodynamics to the acoustic modes of the actual 3D annular duct by means of strip analysis. Other methods can be found in the literature: Kaji and Okazaki (1970) developed a coupled stator/rotor theory which, however, limited the analysis to a single frequency and did not include the swirl effect. On the contrary, the methodology provided by Heinig (1983) may be applied to turbomachines with non-uniform swirling flows. A more accurate 3D analytical model is presented by Posson et al. (2010). Since the 1990s, thanks to the growth in computer technology, "time-linearized" methods have been developed, capable of dealing with real blade geometries and non-uniform mean flows (Hall and Clark (1993); Hall and Lorence (1993); Chassaing and Gerolymos (2000); Campobasso and Giles (2003); Kennepohl et al. (2001)). Such methods were first employed to evaluate the acoustic response of a single blade row, but can also be efficiently used to predict the tone noise emission at the turbine exit by integrating the time-linearized code in a proper propagation procedure (Korte et al. (2005); Pinelli et al. (2011a); Frey et al. (2012)).

In this paper, two different approaches for tonal noise evaluation of a low pressure turbine will be presented. The first one, a preliminary analysis technique, is suitable for the early design phase, whereas the other one, a 3D linearized method, can be used in the last steps of the acoustic design.

The preliminary acoustic tool is able to quickly estimate the tone noise emissions of a multistage LPT. The method is based on simple mean line aerodynamic data and takes into account both acoustic generation and propagation phenomena. For this reason, it can be seen as an extension of Hanson's coupled 2D cascade theory (Hanson (1994)): it extends Hanson's theory for a single fan stage (two rows) to a multi-stage system (turbine). Adjacent blade rows are modeled as 2D flat plate cascades and are included in a fully coupled unsteady analysis, which satisfies the flow tangency boundary condition on both rows simultaneously for several harmonics. In this way noise generation, scattering and reflections are accounted for by solving a large linear system. Further, the swirling flow between adjacent rows is considered by means of actuator disks. Following this approach, the method describes the evolution of the turbine-generated acoustic modes along the machine, and provides for each of them SPL and PWL values at the exhaust section.

On the other hand, the linearized method, already described by the authors in previous works (Arnone et al. (2003); Poli et al. (2006); Boncinelli et al. (2006); Poli et al. (2009)), is based on a fully three-dimensional aeroacoustic solver integrated in a proper propagation strategy (Pinelli et al. (2011b,a)) and can be fruitfully used during the detailed acoustic design.

A wide validation of both tools is reported, based on the experimental database measured in an acoustic test rig, representative of the last stages of a low-pressure turbine. All these activities are carried out in the context of a research project on turbomachinery Computational Aeroelasticity (CA) and Computational Aeroacoustics (CAA) at the Department of Industrial Engineering (University of Florence) in collaboration with Avio S.p.A..

THEORY OF THE NOISE PREDICTION METHODS

This section describes the theoretical basis of the two numerical methods which will be used to predict acoustic emissions of a LPT for aeronautical applications. Special emphasis will be put on the

preliminary analysis tool based on a semi-analytical method; the 3D linearized method will be only briefly presented as it has already been described by the authors in (Pinelli et al. (2011a)).

Preliminary analysis tool

The preliminary analysis tool (named TNT: Tone Noise Tool) is an extension of Hanson's coupled cascade theory from fan to LPT applications, although it is acknowledged that the flat plate assumption is stronger for a turbine environment than for a fan/OGV interaction. Moreover, the method extension allows the analysis not only of the tone noise generation, as did the original theory, but also of the acoustic propagation through successive rows up to turbine exhaust. The tool which was developed computes the interaction between two adjacent blade rows (see right side of figure 1) and estimates either the effect of the wake from the upstream blade rows impinging on the successive blade row *(generation module)*, or the effect of an acoustic wave imposed in the gap between rows *(propagation module)*. These interactions produce unsteady loading on both rows and thereby generate outgoing acoustic waves. The model takes into account reflection/transmission characteristics and the swirling flow between the two rows by means of actuator disk theory. Unlike simpler methods, in which there is a one-to-one relationship between wake harmonics and noise harmonics, the presented method simultaneously couples the effects of multiple harmonics in a large linear system. In this way noise generation, scattering and reflections effects can be included in the model. The solution of the linear system is the unsteady loading distribution on both rows for each harmonic caused by incoming perturbations. Once the unsteady loading is computed, it is simple to derive the resulting output waves in terms of SPL and PWL.

Basic theory

The basis of Hanson's coupled 2D theory is Smith's theory (Smith (1973)). Smith derived a theoretical approach which relates the unsteady loading of a single cascade of flat plates with a specified velocity disturbance entering the system. This approach is based on an integral equation for the upwash velocity (disturbance velocity component normal to the blade chord, see left side of figure 1) on the cascade caused by the unknown load distribution. The resulting equations can be solved for

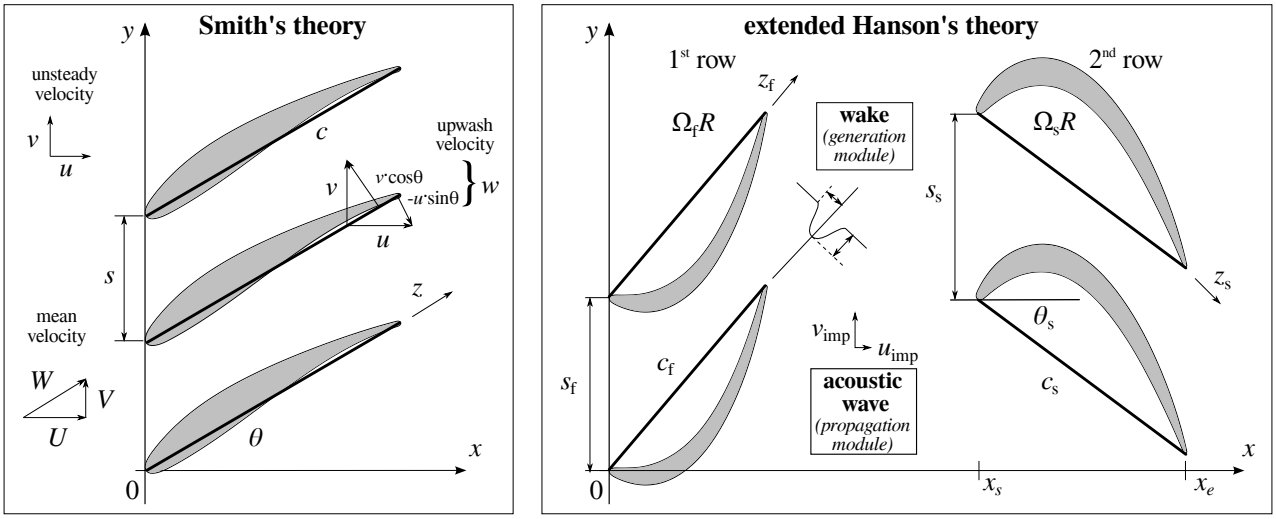

Figure 1: **Geometry of Smith's theory (left) and geometry of coupled cascade (right)**

the loads and hence the outgoing acoustic waves can be evaluated. As usual in acoustics, Smith starts with the linearized differential equations for continuity and momentum and assumes the following

form for velocity and pressure perturbations (complex quantities are marked with the oversign ˜):

$$\begin{bmatrix} u \\ v \\ p \end{bmatrix} = \Re\mathrm{e}\left\{ \begin{bmatrix} \tilde{u} \\ \tilde{v} \\ \tilde{p} \end{bmatrix} e^{\jmath(k_x x + k_y y + \omega t)} \right\} \qquad \text{where} \qquad k_y = \frac{m}{R} \tag{1}$$

This analysis leads to two families of solutions of the continuity and momentum equations: the first family includes the pressure waves, which propagate up/downstream (with or without attenuation) at the speed of sound a, while the second one contains the vorticity waves which are convected downstream by the mean flow. The respective axial wave numbers are given by:

$$k_{x\,1,2} = \frac{U(\omega + Vk_y) \pm a\sqrt{(\omega + Vk_y)^2 - (a^2 - U^2)k_y^2}}{a^2 - U^2} \qquad k_{x\,3} = -\frac{(\omega + Vk_y)}{U} \tag{2}$$

Moreover, the relations between velocity and pressure complex mode amplitudes are:

$$\tilde{u}_{1,2} = k_{x\,1,2}\frac{\tilde{v}_{1,2}}{k_y} \qquad \tilde{p}_{1,2} = -(\omega + Uk_{x\,1,2} + Vk_y)\varrho\frac{\tilde{v}_{1,2}}{k_y} \qquad \text{and} \qquad \tilde{u}_3 = -k_y\frac{\tilde{v}_3}{k_{x\,3}} \tag{3}$$

Smith then deduces equation 4 which describes the total circumferential perturbation velocity related to each wave type.

$$v_{1,2,3}^{(\text{total})} = \int_0^c \Re\mathrm{e}\left\{ \sum_{k=-\infty}^{\infty} v'_{1,2,3}\, e^{\jmath(k_{x\,1,2,3}x + k_y y + \omega t)}\, e^{-\jmath(k_{x\,1,2,3}\cos\theta + k_y \sin\theta)z} \right\} \frac{\Gamma(z)}{s}\,\mathrm{d}z \tag{4}$$

Upstream of the cascade there will be only the $v_1^{(\text{total})}$ component which corresponds to the circumferential velocity perturbation due to all upstream running pressure waves. In the same way, anywhere downstream of the row, $v_2^{(\text{total})}$ (sum of downstream running pressure waves) and $v_3^{(\text{total})}$ (sum of vorticity waves) will be present. Expressions for v'_1, v'_2 and v'_3 are directly derived from Smith's theory (see Smith (1973)) and respectively represent the influence of a unit loading element on the up/downstream running pressure and vorticity waves. Then, the load distribution over the blade chord is discretized into N_p identical panels and the integral is converted to a sum according to:

$$\frac{1}{c}\int_{z_j - \frac{\Delta z}{2}}^{z_j + \frac{\Delta z}{2}} \frac{\Gamma(z)}{W}\,\mathrm{d}z \implies \mathscr{L}(j) \qquad \text{where} \qquad \Delta z = \frac{c}{N_p} \tag{5}$$

Following Hanson's approach equation 4 can thus be generalized for each row with multiple harmonics for any wave type:

$$v^{(\text{total})} = \frac{W}{s/c}\sum_{k_{\mathrm{f,s}}=-\infty}^{+\infty}\sum_{i=1}^{N_p} \Re\mathrm{e}\left\{ \sum_{k_{\mathrm{s,f}}=-\infty}^{+\infty} v'\, e^{\jmath(k_x x + k_y y + \omega t)}\, e^{-\jmath(k_x\cos\theta + k_y\sin\theta)z_i} \right\} \times \mathscr{L}(k_{\mathrm{f,s}}, i) \tag{6}$$

Wave system

The next step is to derive the form of all the waves which can result from a generic interaction between adjacent rows for both generation and propagation cases. When dealing with a wave generation phenomenon, the classical Tyler and Sofrin spinning modes are generated. Such modes form the wave system for the *generation module* and are described in the fixed reference frame in the left side of equations 7.

$$\underbrace{\begin{aligned} m &= k_{\mathrm{s}}N_{\mathrm{s}} - k_{\mathrm{f}}N_{\mathrm{f}} \\ \omega &= k_{\mathrm{f}}N_{\mathrm{f}}\Omega_{\mathrm{f}} - k_{\mathrm{s}}N_{\mathrm{s}}\Omega_{\mathrm{s}} \end{aligned}}_{(generation\ module)} \qquad \underbrace{\begin{aligned} m &= m_0 + k_{\mathrm{f}}N_{\mathrm{f}} + k_{\mathrm{s}}N_{\mathrm{s}} \\ \omega &= \omega_0 - k_{\mathrm{f}}N_{\mathrm{f}}\Omega_{\mathrm{f}} - k_{\mathrm{s}}N_{\mathrm{s}}\Omega_{\mathrm{s}} \end{aligned}}_{(propagation\ module)} \tag{7}$$

The present extension of Hanson's theory also allows the propagation of a single mode through successive rows (one at a time, together with the previously analyzed row). This means that the wave system describing the propagation problem is different and has to be composed of the imposed wave (with m_0 and ω_0) together with all the scattering modes due to the two blade rows. The wave system for the *propagation module* is depicted by the right side of equations 7. The same conclusion was drawn by Hall et al. (2006) in their work on flutter in a multistage environment. Furthermore, if the imposed wave (with m_0 and ω_0) is a vector of turbulence modes, right side of equations 7 also describe the set of permitted broadband modes (see Hanson (2001)).

Reflection and transmission coefficients

Swirling flow between rows must be considered in order to have a better representation of the mean flow properties. As explained in Hanson (1994), actuator disks can be used to turn the mean flow at the 1st row leading edge and at the 2nd row trailing edge (see figure 2). As the mean flow changes across the inlet and exit interfaces, the unsteady quantities vary as well. This can be handled by employing reflection $\mathcal{R}$ and transmission $\mathcal{T}$ coefficients for all the waves. Such coefficients are directly derived from the linearized continuity of mass and momentum .

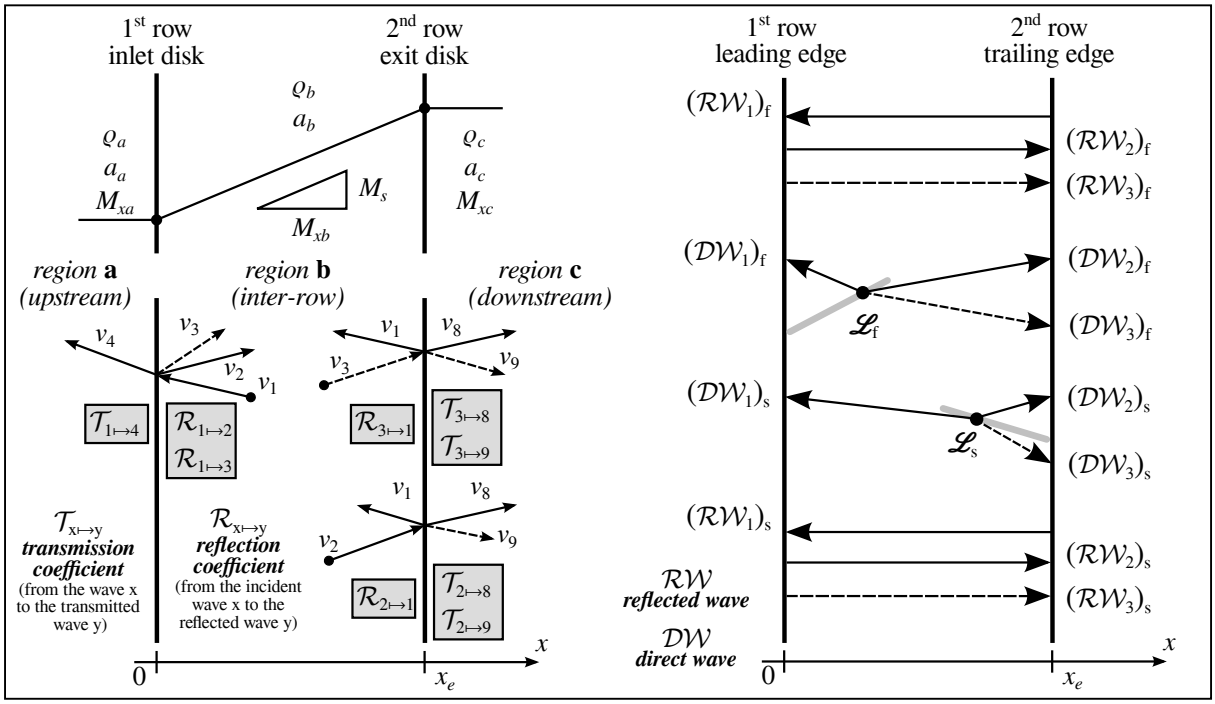

Figure 2: **Coupled theory: reflection/transmission coefficients (left), waves system (right)**

Coupled 2D theory

In order to couple the problem, it is sufficient to construct the wave field between the 1st row leading edge and the 2nd row trailing edge by means of direct waves coming from each loading element (via Smith's formulae) plus the waves reflected from the inlet and exit interfaces (see figure 2). For a loading element of the 1st row, for instance, the direct waves $(\mathcal{DW}_{1,2,3})_{\mathrm{f}}$ from each panel are obtained by Smith's theory, while the reflected waves $(\mathcal{RW}_{1,2,3})_{\mathrm{f}}$ can be built as follows:

$$
\begin{aligned}
(\mathcal{RW}_1)_{\mathrm{f}} &= [(\mathcal{DW}_2)_{\mathrm{f}} + (\mathcal{RW}_2)_{\mathrm{f}}]\,\mathcal{R}_{2\to1} + [(\mathcal{DW}_3)_{\mathrm{f}} + (\mathcal{RW}_3)_{\mathrm{f}}]\,\mathcal{R}_{3\to1} \\
(\mathcal{RW}_2)_{\mathrm{f}} &= [(\mathcal{DW}_1)_{\mathrm{f}} + (\mathcal{RW}_1)_{\mathrm{f}}]\,\mathcal{R}_{1\to2} \\
(\mathcal{RW}_3)_{\mathrm{f}} &= [(\mathcal{DW}_1)_{\mathrm{f}} + (\mathcal{RW}_1)_{\mathrm{f}}]\,\mathcal{R}_{1\to3}
\end{aligned}
\tag{8}
$$

and similar equations hold for the 2nd row. Such coupling equations are written in terms of transverse velocity $v_{1,2,3}$ components. Now, the axial velocity $u_{1,2,3}$ can be obtained by using equation 3, so that it is straightforward to derive the upwash velocity (see Hanson (1994)). Together, all the coupling equations (such as equations 6 and 8) written in terms of upwash velocity, define four sub-matrices of influence, and sub-matrices can be assembled into a large matrix representing the entire coupled system.

$$\begin{bmatrix} \mathscr{K}_{\mathrm{f}\to\mathrm{f}} & \mathscr{K}_{\mathrm{s}\to\mathrm{f}} \\ \mathscr{K}_{\mathrm{f}\to\mathrm{s}} & \mathscr{K}_{\mathrm{s}\to\mathrm{s}} \end{bmatrix} \times \begin{bmatrix} \mathscr{L}_{\mathrm{f}} \\ \mathscr{L}_{\mathrm{s}} \end{bmatrix} = \begin{bmatrix} \mathscr{W}_{\mathrm{f}} \\ \mathscr{W}_{\mathrm{s}} \end{bmatrix} \tag{9}$$

When dealing with the *propagation module* of the acoustic tool, the deeper structure of the coupled linear system, for the special case of $-1 < k_{\mathrm{f,s}} < +1$, becomes as shown in equation 10.
Inside this large system each sub-matrix includes the kernel quantity for each element discretizing the two rows. It is worth noting how the system explicitly shows the modal and frequency scattering and how it allows the inclusion of multiple reflections between the rows.

$$\begin{bmatrix}
\begin{bmatrix} \mathscr{K}_{\mathrm{f}\to\mathrm{f}} \\ k_{\mathrm{f}}=-1 \\ k_{\mathrm{s}}=-1 \end{bmatrix} & \begin{bmatrix} 0 \end{bmatrix} & \begin{bmatrix} 0 \end{bmatrix} & \begin{bmatrix} \mathscr{K}_{\mathrm{s}\to\mathrm{f}} \\ k_{\mathrm{f}}=-1 \\ k_{\mathrm{s}}=-1 \end{bmatrix} & \begin{bmatrix} \mathscr{K}_{\mathrm{s}\to\mathrm{f}} \\ k_{\mathrm{f}}=0 \\ k_{\mathrm{s}}=-1 \end{bmatrix} & \begin{bmatrix} \mathscr{K}_{\mathrm{s}\to\mathrm{f}} \\ k_{\mathrm{f}}=+1 \\ k_{\mathrm{s}}=-1 \end{bmatrix} \\
\begin{bmatrix} 0 \end{bmatrix} & \begin{bmatrix} \mathscr{K}_{\mathrm{f}\to\mathrm{f}} \\ k_{\mathrm{f}}=0 \\ k_{\mathrm{s}}=0 \end{bmatrix} & \begin{bmatrix} 0 \end{bmatrix} & \begin{bmatrix} \mathscr{K}_{\mathrm{s}\to\mathrm{f}} \\ k_{\mathrm{f}}=-1 \\ k_{\mathrm{s}}=0 \end{bmatrix} & \begin{bmatrix} \mathscr{K}_{\mathrm{s}\to\mathrm{f}} \\ k_{\mathrm{f}}=0 \\ k_{\mathrm{s}}=0 \end{bmatrix} & \begin{bmatrix} \mathscr{K}_{\mathrm{s}\to\mathrm{f}} \\ k_{\mathrm{f}}=+1 \\ k_{\mathrm{s}}=0 \end{bmatrix} \\
\begin{bmatrix} 0 \end{bmatrix} & \begin{bmatrix} 0 \end{bmatrix} & \begin{bmatrix} \mathscr{K}_{\mathrm{f}\to\mathrm{f}} \\ k_{\mathrm{f}}=+1 \\ k_{\mathrm{s}}=+1 \end{bmatrix} & \begin{bmatrix} \mathscr{K}_{\mathrm{s}\to\mathrm{f}} \\ k_{\mathrm{f}}=-1 \\ k_{\mathrm{s}}=+1 \end{bmatrix} & \begin{bmatrix} \mathscr{K}_{\mathrm{s}\to\mathrm{f}} \\ k_{\mathrm{f}}=0 \\ k_{\mathrm{s}}=+1 \end{bmatrix} & \begin{bmatrix} \mathscr{K}_{\mathrm{s}\to\mathrm{f}} \\ k_{\mathrm{f}}=+1 \\ k_{\mathrm{s}}=+1 \end{bmatrix} \\
\begin{bmatrix} \mathscr{K}_{\mathrm{f}\to\mathrm{s}} \\ k_{\mathrm{f}}=-1 \\ k_{\mathrm{s}}=-1 \end{bmatrix} & \begin{bmatrix} \mathscr{K}_{\mathrm{f}\to\mathrm{s}} \\ k_{\mathrm{f}}=0 \\ k_{\mathrm{s}}=-1 \end{bmatrix} & \begin{bmatrix} \mathscr{K}_{\mathrm{f}\to\mathrm{s}} \\ k_{\mathrm{f}}=+1 \\ k_{\mathrm{s}}=-1 \end{bmatrix} & \begin{bmatrix} \mathscr{K}_{\mathrm{s}\to\mathrm{s}} \\ k_{\mathrm{f}}=-1 \\ k_{\mathrm{s}}=-1 \end{bmatrix} & \begin{bmatrix} 0 \end{bmatrix} & \begin{bmatrix} 0 \end{bmatrix} \\
\begin{bmatrix} \mathscr{K}_{\mathrm{f}\to\mathrm{s}} \\ k_{\mathrm{f}}=-1 \\ k_{\mathrm{s}}=0 \end{bmatrix} & \begin{bmatrix} \mathscr{K}_{\mathrm{f}\to\mathrm{s}} \\ k_{\mathrm{f}}=0 \\ k_{\mathrm{s}}=0 \end{bmatrix} & \begin{bmatrix} \mathscr{K}_{\mathrm{f}\to\mathrm{s}} \\ k_{\mathrm{f}}=+1 \\ k_{\mathrm{s}}=0 \end{bmatrix} & \begin{bmatrix} 0 \end{bmatrix} & \begin{bmatrix} \mathscr{K}_{\mathrm{s}\to\mathrm{s}} \\ k_{\mathrm{f}}=0 \\ k_{\mathrm{s}}=0 \end{bmatrix} & \begin{bmatrix} 0 \end{bmatrix} \\
\begin{bmatrix} \mathscr{K}_{\mathrm{f}\to\mathrm{s}} \\ k_{\mathrm{f}}=-1 \\ k_{\mathrm{s}}=+1 \end{bmatrix} & \begin{bmatrix} \mathscr{K}_{\mathrm{f}\to\mathrm{s}} \\ k_{\mathrm{f}}=0 \\ k_{\mathrm{s}}=+1 \end{bmatrix} & \begin{bmatrix} \mathscr{K}_{\mathrm{f}\to\mathrm{s}} \\ k_{\mathrm{f}}=+1 \\ k_{\mathrm{s}}=+1 \end{bmatrix} & \begin{bmatrix} 0 \end{bmatrix} & \begin{bmatrix} 0 \end{bmatrix} & \begin{bmatrix} \mathscr{K}_{\mathrm{s}\to\mathrm{s}} \\ k_{\mathrm{f}}=+1 \\ k_{\mathrm{s}}=+1 \end{bmatrix}
\end{bmatrix} \times \begin{bmatrix}
\begin{bmatrix} \mathscr{L}_{\mathrm{f}} \\ k_{\mathrm{f}}=-1 \end{bmatrix} \\
\begin{bmatrix} \mathscr{L}_{\mathrm{f}} \\ k_{\mathrm{f}}=0 \end{bmatrix} \\
\begin{bmatrix} \mathscr{L}_{\mathrm{f}} \\ k_{\mathrm{f}}=+1 \end{bmatrix} \\
\begin{bmatrix} \mathscr{L}_{\mathrm{s}} \\ k_{\mathrm{s}}=-1 \end{bmatrix} \\
\begin{bmatrix} \mathscr{L}_{\mathrm{s}} \\ k_{\mathrm{s}}=0 \end{bmatrix} \\
\begin{bmatrix} \mathscr{L}_{\mathrm{s}} \\ k_{\mathrm{s}}=+1 \end{bmatrix}
\end{bmatrix} = \begin{bmatrix}
\begin{bmatrix} \mathscr{W}_{\mathrm{f}} \\ k_{\mathrm{f}}=-1 \end{bmatrix} \\
\begin{bmatrix} \mathscr{W}_{\mathrm{f}} \\ k_{\mathrm{f}}=0 \end{bmatrix} \\
\begin{bmatrix} \mathscr{W}_{\mathrm{f}} \\ k_{\mathrm{f}}=+1 \end{bmatrix} \\
\begin{bmatrix} \mathscr{W}_{\mathrm{s}} \\ k_{\mathrm{s}}=-1 \end{bmatrix} \\
\begin{bmatrix} \mathscr{W}_{\mathrm{s}} \\ k_{\mathrm{s}}=0 \end{bmatrix} \\
\begin{bmatrix} \mathscr{W}_{\mathrm{s}} \\ k_{\mathrm{s}}=+1 \end{bmatrix}
\end{bmatrix} \tag{10}$$

The last point to address is the determination of the upwash array $\mathscr{W}$: this can be done by imposing the no-through-flow boundary condition on both rows. Different conditions must be applied to the two rows. At the 1st row, the sum of upwash caused by the row itself and 2nd row is always zero except for the case of upstream pressure propagation *(propagation module)*, where $\mathscr{W}$ is the opposite of the upwash due to the imposed pressure wave impinging on the 1st row. On the other hand, the upwash on the 2nd row is zero only for upstream pressure propagation while, in any other case, it is caused either by viscous wake *(generation module)* or by downstream running pressure wave *(propagation module)*.

$$\begin{bmatrix} \mathscr{W}_{\mathrm{f}} \\ \mathscr{W}_{\mathrm{s}} \end{bmatrix} = \begin{bmatrix} \mathscr{W}_{\mathrm{f}\to\mathrm{f}} + \mathscr{W}_{\mathrm{s}\to\mathrm{f}} \\ \mathscr{W}_{\mathrm{f}\to\mathrm{s}} + \mathscr{W}_{\mathrm{s}\to\mathrm{s}} \end{bmatrix} = \underbrace{\begin{bmatrix} 0 \\ -\mathscr{W}_{wake} \end{bmatrix}}_{(generation\ module)} \text{ or } \underbrace{\begin{bmatrix} -\mathscr{W}_{up} \\ 0 \end{bmatrix} \text{ or } \begin{bmatrix} 0 \\ -\mathscr{W}_{down} \end{bmatrix}}_{(propagation\ module)} \tag{11}$$

The *generation module* of the tool requires knowing the wake defect generated by the 1st row in order to obtain $\mathscr{W}_{wake}$. For this purpose, a viscous wake correlation is used. In a different way, the upwash $\mathscr{W}_{up}$ or $\mathscr{W}_{down}$ for the *propagation module* is basically composed of the normal components of u, v associated with the up/downstream running pressure wave to be propagated. Obviously, u, v come from a previous generation or propagation analysis.

Solving the coupled system

Once the large matrix describing the generation or propagation problem has been filled in and the upwash vector has been built, the unsteady load can be computed by solving the linear system. To efficiently do this, the optimized LAPACK library (Anderson et al. (1999)) routine based on the LU factorization in OpenMP parallelism was chosen. Now, for acoustic purposes, it is necessary to derive the SPL of each acoustic wave generated by the unsteady load of both rows in upstream and downstream regions. This can be accomplished by using the transmission coefficients $\mathcal{T}$ and then equations 3. Finally, to obtain the PWL, the classical formula of the acoustic intensity projected in axial direction can be used.

$$\vec{I} = \left(\frac{p}{\varrho} + \vec{w}\cdot\vec{W}\right)\left(\varrho\vec{w} + \rho\vec{W}\right) \quad \Longrightarrow \quad I_x = \vec{I}\cdot\vec{i_x} = \left(\frac{p}{\varrho} + Uu + Vv\right)\left(\varrho u + \frac{p}{a^2}U\right) \tag{12}$$

The acoustic power $\mathcal{W}$ is the time average of I_x integrated over the duct cross sectional area A. Since the concept of duct area is not defined in this 2D analysis, it is appropriate to compute the average power per unit area, as follows:

$$\frac{\mathcal{W}}{A} = \frac{1}{2\pi}\int_0^{2\pi}\frac{1}{T}\int_0^T I_x \,\mathrm{d}t\,\mathrm{d}\phi \qquad \text{where } \phi \text{ is the longitudinal angle} \tag{13}$$

Fully 3D linearized method

The 3D method for acoustic prediction is based on a time-linearized aeroelastic and aeroacoustic solver named Lars. The Lars code is able to deal with incoming perturbations due to unsteady interactions with upstream/downstream rows (tone noise) which are treated with a non-reflecting boundary condition approach based on radial mode decomposition (Poli et al. (2009)).

For the numerical evaluation of the tone noise reaching the turbine exit, both generation and propagation phenomena have to be properly simulated and, for this reason, the single blade aeroacoustic solver was integrated into a proper propagation procedure. Generation of the sound is handled by means of a wave splitting method, while the propagation method consists of a sequence of linearized aeroacoustic computations, which transmit the most relevant waves in the propagation direction. Moreover, to have a better insight of the physical mechanisms which govern certain behaviors, the propagation analysis has necessarily to account for the 3D physics of waves in annular ducts. Hence, it is important that the propagation strategy follow the evolution of each acoustic mode from its source up to the engine exit, taking into account the radial shape of the traveling perturbations. The procedure developed by the authors may be applied to both downstream and upstream running waves, and is suitable for turbine as well as compressor/fan applications. Further details of this method can be found in Pinelli et al. (2011a).

ACOUSTIC TEST RIG

Engine noise measurements usually provide overall qualitative information on propagating turbine tones and associated noise levels: engine acoustic data are representative of the whole propulsion system, and the rear arc spectrum includes several acoustic contributions as well as installation effects. For this reason, the identification of turbine emissions is not straightforward and is mainly based on frequency and directivity data. In this context, a cold flow rig becomes a very attractive way to gain a deeper physical understanding, and to have a high-quality, detailed dataset for a direct and complete validation of noise generation and in-duct propagation tools. Acoustic cold flow measurements provide a relation between acquired acoustic data and the generating turbine. The identification of the LPT acoustic emissions is based on the circumferential and radial mode order detection technique.

Starting from the above considerations, an acoustic cold flow rig (Taddei et al. (2009)) has been recently set up at Avio (see figure 3). The acoustic measurements coming from first test campaigns have already been used for CAA validation (Pinelli et al. (2011a)), generally highlighting a good agreement between numerical prediction and experimental data.

Figure 3: **Cold flow rig (left), 1st vane geometry with instrumented blades removed (right) and kulite rake (box)**

The Avio annular rig has a modular design which allows easy replacement of rows, variation of row axial spacing and addition of rows (inlet or outlet guide vanes, single-stage to two-stage setups). In designing the model turbine, engine-to-rig similitude criteria have been followed (such as Mach number similarity): blade geometries, loadings and flow deflections have been selected according to state-of-the-art design of a commercial aeroengine LPT, while the airfoil count provides aeroacoustic similitude in terms of reduced frequency. The rig operates at ambient exit pressure and the overpressure at inlet is provided by a compressor. A flat endwall geometry was chosen, which is representative of the turbine rear stages and allows for easy rig assembly.

Concerning measurement capabilities, both aerodynamic and acoustic instrumentation have been installed. The aerodynamic instrumentation is aimed at characterizing the turbine operating conditions and resolving the mean flow field at turbine inlet and outlet. As far as the noise measurements are concerned, a rotating duct at turbine exit has been introduced to permit the detailed mapping of the generated acoustic field and its propagation pattern by means of two kulite rakes. Other measurement devices are available in the cold flow, i.e. axial arrays of flush-mounted microphones. Currently the microphones are used for confirmation of the kulite measurements in the mid-low frequency range. The azimuthal positioning system allows for collecting of a sufficient number of acoustic pressure data along the circumferential direction to detect all relevant cut-on modes at the various flow conditions (namely approach and cutback conditions, plus other additional operating points). High speed acquisition hardware is used, allowing the simultaneous acquisition of all unsteady pressure signals. Additionally, a one pulse per revolution is recorded to allow synchronous re-sampling of pressure signals, aimed at increasing the signal-to-noise ratio and avoiding detrimental effects due to rotor speed variations (hence improving the global accuracy of the analysis). Finally, based on the acoustic field mapping, complemented by flow field description, modal decomposition techniques (extended to account for swirling flow) have been applied and propagating modes detected. The comparisons described in the following section refer to an experimental campaign where a two-stage turbine was tested with the addition of a leaned Turbine Rear Frame (TRF).

LPT TONE NOISE RESULTS

In the following, selected comparisons between experimental and numerical results of the acoustic test rig at the approach configuration will be presented and discussed. This operating point was chosen since it turns out to be the most critical for LPT tone noise emissions. At the time of writing, different operating conditions and turbine setups are still under investigation.

Comparison between experimental and numerical results

The measured acoustic spectrum at turbine exhaust for approach conditions has been processed by RMA (Radial Mode Analysis, see Taddei et al. (2009)) to show the modal content of the acoustic pressure field for each selected frequency. The results highlight a pronounced relevance of peaks caused by the rotor-stator interactions, especially at the 1st blade passing frequency (BPF) of the first rotor, since the V1-B1 interaction is designed for being cut-on. These peaks are connected to the generating interactions by means of a circumferential analysis. In this way, the relevant interactions (reported in figure 4) can be identified and then analyzed numerically.

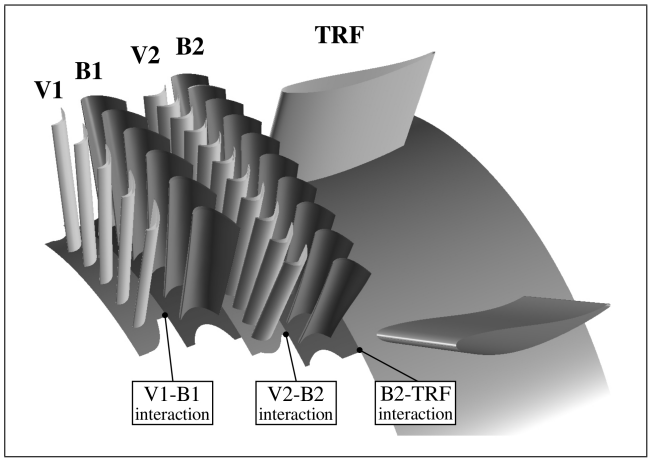

Figure 4: **Cold flow rig: geometry of the rows**

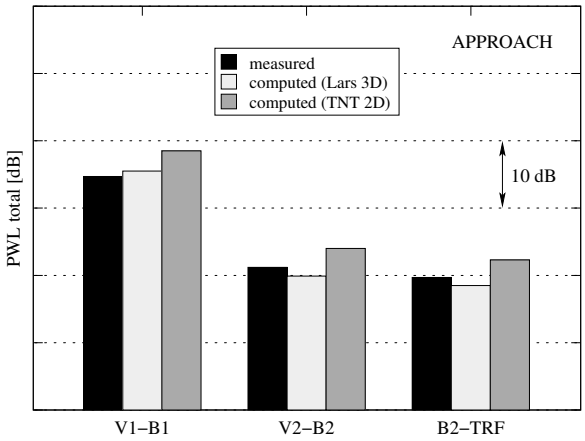

Figure 5: **Total PWL at the turbine exhaust**

The three interactions being analyzed have different behaviors inside the turbine (cut-on/cut-off), yet they all produce a lot of cut-on waves at the TRF exit. A comparison of total PWL emissions of such interactions are shown in figure 5. As can be seen, the agreement is very good and the differences between measurements and 3D calculations are within 1.5 dB. The mesh dimensions used for the 3D

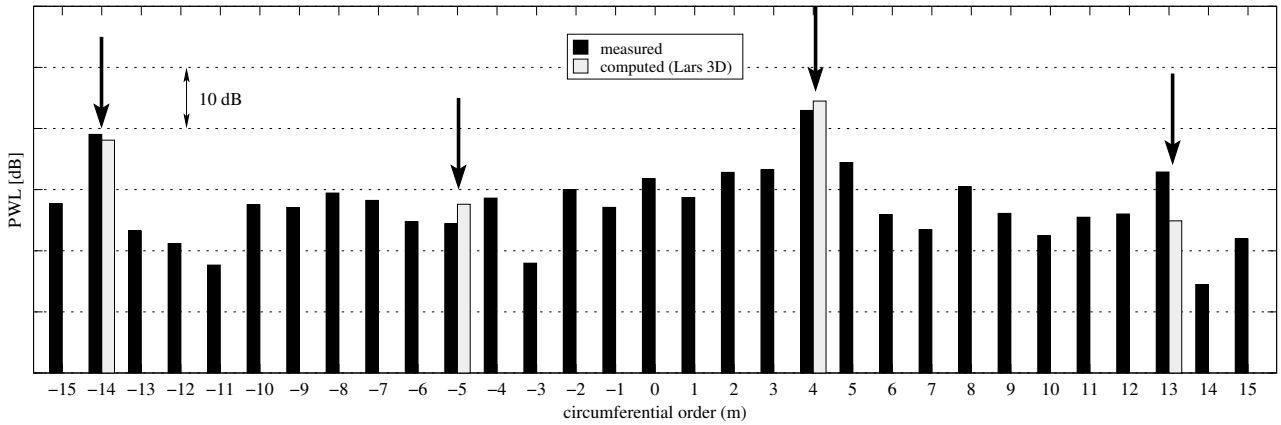

Figure 6: **Modal decomposition results for the 1st BPF (B1) at the turbine exit**

calculations are approximately $180\times100\times80$ for each inter-blade vane, ensuring at least 30 cells per convected wavelength and 70 cell per acoustic wavelength. However, the preliminary design tool results also agree well with the measurements, despite the strong assumption of flat plate geometries, which could be a possible source of discrepancy. This approach tends to overestimate the emissions: this may also be due to the fact that the 2D tool computes an average power per unit area, which is then considered constant over the duct area to get the total PWL. However, this simplified method is able to reproduce the correct relative relevance of the studied emissions, confirming its usefulness in the early steps of machine design. For each BPF, the total power at TRF exit can be split up into modal orders to highlight the effect of TRF scattering. Figure 6 shows the modal decomposition for the 1st BPF of the first rotor. The arrows indicate the components related to the V1-B1 interaction in comparison to the 3D results after the scattering effect of the TRF. Measurements and numerical predictions are in really good agreement. Analogous considerations can be made for the modal results at the 1st BPF of the second rotor, showing the V2-B2 and B2-TRF interactions. This mode splitting

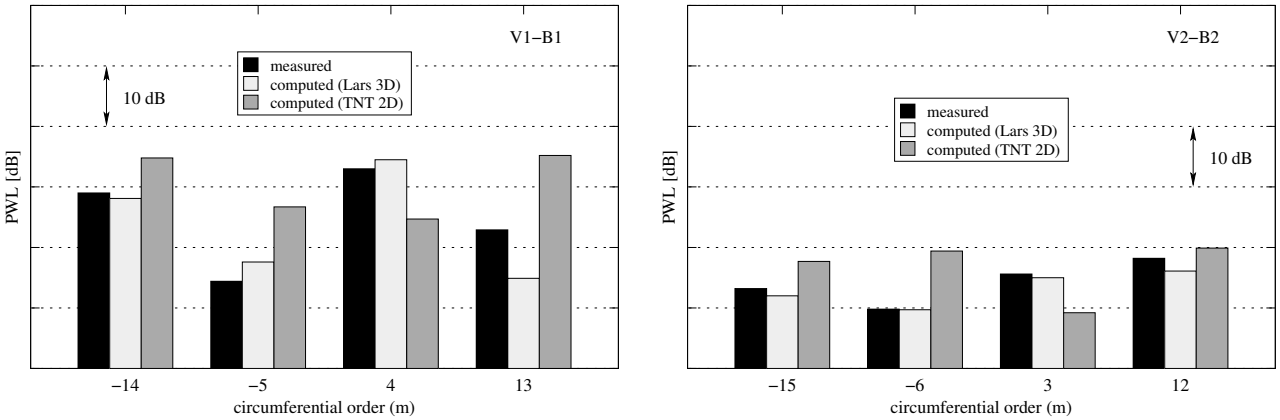

Figure 7: **Comparison of modal components: V1-B1 (left) and V2-B2 (right)**

was also computed by the preliminary tool and the results for V1-B1 and V2-B2 interactions are summarized in figure 7. As expected, the 3D method, which is able to account for the radial shape of acoustic perturbations, gives a better agreement with measurements in terms of PWL splitting, with respect to the preliminary analysis tool.

CONCLUSIONS

Two prediction methods for LPT tone noise emissions have been presented: an analytic tool aimed at the preliminary evaluation of the LPT acoustic design, and a 3D CAA linearized approach suitable for the detailed design phase. The acoustic predictions provided by both methods have been compared to the experimental results coming from an acoustic test campaign carried out on a cold flow rig at Avio: the highlighted agreement is very good, especially for the 3D results. This demonstrates the prediction capability of the methods and confirms their usefulness as design tools.

ACKNOWLEDGMENTS

The authors would like to acknowledge Avio S.p.A. for the financial support and the permission to publish. Special thanks to Dr. Francesco Taddei (Department of Industrial Engineering, University of Florence) for his useful technical contribution.

REFERENCES

Amiet, R. (1974). Transmission and reflection of sound by two blade rows. *Journal of Sound and Vibration*, 34 (3):399–412.

Anderson, E., Bai, Z., Bischof, C., Blackford, S., Demmel, J., Dongarra, J., Croz, J. D., Greenbaum, A., Hammarling, S., McKenney, A., and Sorensen, D. (1999). *LAPACK Users' Guide*. Society for Industrial and Applied Mathematics, Philadelphia, PA, third edition.

Arnone, A., Poli, F., and Schipani, C. (2003). A method to assess flutter stability of complex modes. In 10^{th} *International Symposium on Unsteady Aerodynamics, Aeroacoustics and Aeroelasticity of Turbomachines*.

Boncinelli, P., Marconcini, M., Poli, F., Arnone, A., and Schipani, C. (2006). Time-linearized quasi-3D tone noise computations in cascade flows. In *IGTI ASME Turbo Expo*. ASME paper GT2006-90080.

Campobasso, M. and Giles, M. (2003). Effects of flow instabilities on the linear analysis of turbomachinery aeroelasticity. *Journal of propulsion and power*, 19(2):250–259.

Chassaing, J.-C. and Gerolymos, G. (2000). Compressor flutter analysis using time-nonlinear and time-linearized 3-D Navier-Stokes methods. In 9^{th} *International Symposium on Unsteady Aerodynamics, Aeroacoustics and Aeroelasticity of Turbomachines*.

Frey, C., Ashcroft, G., Kersken, H., and Weckmüller, C. (2012). Advanced numerical methods for the prediction of tonal noise in turbomachinery, part II: Time-linearized methods. In *IGTI ASME Turbo Expo*. ASME paper GT2012-69418.

Hall, K. and Clark, W. (1993). Linearized Euler predictions of unsteady aerodynamic loads in cascades. *AIAA Journal*, 31:540–550.

Hall, K., Ekici, K., and Voytovych, D. (2006). Multistage coupling for unsteady flows in turbomachinery. In *Unsteady Aerodynamics, Aeroacoustics and aeroelasticity of turbomachines*, pages 217–229. Springer Netherlands.

Hall, K. and Lorence, C. (1993). Calculation of three-dimensional unsteady flows in turbomachinery using the linearized harmonic Euler equations. *Transactions of the ASME, Journal of turbomachinery*, 115:800–809.

Hanson, D. (1994). Coupled 2-dimensional cascade theory for noise and unsteady aerodynamics of blade row interaction in turbofans. Volume 1 – Theory development and parametric studies. Technical report, NASA Contractor Report 4506.

Hanson, D. (2001). Broadband noise of fans – with unsteady coupling theory to account for rotor and stator reflection/transmission effects. Technical report, NASA Contractor Report 211136.

Heinig, K. (1983). Sound propagation in multistage axial flow turbomachines. *AIAA Journal*, 15:98–105.

Kaji, S. and Okazaki, T. (1970). Generation of sound by rotor–stator interation. *Journal of Sound and Vibration*, 13(3):281–307.

Kennepohl, F., Kahl, G., and Heinig, K. (2001). Turbine blade/vane interaction noise: Calculation with a 3D time-linearised Euler method. In 7^{th} *AIAA/CEAS Aeroacoustic Conference*.

Koch, W. (1971). On the transmission of sound waves through a blade row. *Journal of Sound and Vibration*, 18 (1):111–128.

Korte, D., Hüttl, T., Kennepohl, F., and Heinig, K. (2005). Numerical simulation of a multistage turbine sound generation and propagation. *Aerospace science and tecnology*, 9:125–134.

Pinelli, L., Poli, F., Marconcini, M., Arnone, A., Spano, E., and Torzo, D. (2011a). Validation of a 3d linearized method for turbomachinery tone noise analysis. In *IGTI ASME Turbo Expo*. ASME paper GT2011-45886.

Pinelli, L., Poli, F., Marconcini, M., Arnone, A., Spano, E., Torzo, D., and Schipani, C. (2011b). A linearized method for tone noise generation and propagation analysis in a multistage contra-rotating turbine. In 9^{th} *European Conference on Turbomachinery Fluid Dynamics and Thermodynamics*.

Poli, F., Arnone, A., and Schipani, C. (2009). A 3D linearized method for turbomachinery tone noise analysis with 3D non-reflecting boundary conditions. In 8^{th} *European Conference on Turbomachinery Fluid Dynamics and Thermodynamics*.

Poli, F., Gambini, E., Arnone, A., and Schipani, C. (2006). A 3D time-linearized method for turbomachinery blade flutter analysis. In 11^{th} *International Symposium on Unsteady Aerodynamics, Aeroacoustics and Aeroelasticity of Turbomachines*.

Posson, H., Roger, M., and Moreau, S. (2010). On a uniformly valid analytical rectilinear cascade response function. *Journal of Fluid Mechanics*, 663:22–52.

Smith, N. (1973). Discrete frequency sound generation in axial flow turbomachines. Technical report. Report R. & M. n^{o} 3709.

Taddei, F., Cinelli, C., De Lucia, M., and Schipani, C. (2009). Experimental investigation of low pressure turbine noise: Radial mode analysis for swirling flows. In 12^{th} *International Symposium on Unsteady Aerodynamics, Aeroacoustics and Aeroelasticity of Turbomachines*.

Tyler, J. and Sofrin, T. (1962). Axial flow compressor noise studies. *Trans. Society of Automotive Engineers*, 70:309–332.

Ventres, C., Theobald, M., and Mark, W. (1982). Turbofan noise generation, vol. I: Analysis. Technical report, NASA Contractor Report 167952.